Invited Paper

Development of silicon-on-insulator waveguide technology

Timo Aalto*[a], Mikko Harjanne[b], Markku Kapulainen[a], Päivi Heimala[a], and Matti Leppihalme[a,b]

[a] VTT Information Technology, Microelectronics,
P.O. Box 1208 (Tietotie 3, Espoo), FIN-02044 VTT, Finland;

[b] Helsinki University of Technology, Optoelectronics laboratory,
P.O. Box 3000 (Tietotie 3, Espoo), FIN-02015 HUT, Finland;

ABSTRACT

An overview of the present silicon-on-insulator (SOI) waveguide technology is given and supplemented with an extensive set of theory and simulation results. Characteristics of slab-, rectangular- and ridge waveguides in SOI are explained. In particular, the number of modes and the single-mode conditions are carefully analyzed. Experimental work with straight and bent 8 to 10 μm thick SOI ridge waveguides and a very fast thermo-optical switch are reported. Propagation loss in a very long spiral waveguide down to 0.3 dB/cm, waveguide birefringence below 10^{-4}, and a switching frequency up to 167 kHz were obtained. A very promising multi-step patterning principle for SOI waveguides is described together with many practical application examples.

Keywords: Silicon-on-insulator, SOI, waveguide, ridge waveguide, thermo-optical switch, polarization, polarization extinction ratio, birefringence

1. INTRODUCTION

Silicon-on-insulator (SOI) waveguides, and high refractive index difference waveguides in general, are very promising for realizing dense photonic integrated circuits (PICs)[1]. They allow extreme miniaturization of PICs due to their ability to realize e.g. ultra small bends, high optical insulation between adjacent waveguides and photonic crystal (PhC) structures[2,3]. SOI waveguides particularly have the advantage of using mature silicon processing technology, and the potential for monolithic integration with electrical and micromechanical structures. SOI waveguide technology is competitive also in less miniaturized and directly fiber coupled telecommunication circuits, where the single mode behavior of large SOI ridge waveguides[4] can be exploited. Such large SOI waveguides have been used to demonstrate e.g. directional and MMI couplers[5], wavelength multiplexers[6], and waveguide gratings[7,8]. High thermal conductivity of silicon can be exploited to make thermo-optic (TO) switches for frequencies well above the typical 1 kHz limit of todays commercial TO switches. A new interferometric modulation technique has been proposed to accelerate TO switches in SOI up to 167 kHz[9]. Fast TO switches based on SOI waveguides can provide a low-cost solution for the optical access networks and the fiber-to-the-home applications. A multi-step patterning principle has been proposed[10] to solve many of the remaining problems in SOI waveguide technology. It can be used to couple light efficiently between various types of waveguides and fibers with different sizes and refractive index distributions. It also enables the realization of highly miniaturized, single moded, and low-loss PICs with reduced processing and packaging costs.

An SOI waveguide has a silicon core ($n \approx 3.5$) surrounded by some cladding material(s), such as air, thermal oxide or deposited oxide, that have n typically between 1 and 2. Therefore, the silicon core always has a very high index difference with respect to the cladding and only a thin cladding layer is needed to insulate the waveguide core from its

* timo.aalto@vtt.fi; phone +358-9-456 6694; fax +358-9-456 7012; http://www.vtt.fi/tte/research/tte6/

Integrated Optics: Devices, Materials, and Technologies VIII,
edited by Yakov Sidorin, Ari Tervonen, Proceedings of SPIE Vol. 5355
(SPIE, Bellingham, WA, 2004) · 0277-786X/04/$15.00 · doi: 10.1117/12.537540

surrounding structures, such as the silicon substrate or any metallic electrodes. In case of standard SOI wafers, there is a buried oxide (BOX) layer between the silicon core and an underlying silicon substrate. Three basic SOI waveguide structures are presented schematically in Fig. 1: a one-dimensional (1D) slab waveguide, a two-dimensional (2D) rectangular waveguide and a 2D ridge waveguide. The very high refractive index difference sets strict requirements for the fabrication technology, especially when the dimensions are small. Single-moded (SM) rectangular SOI waveguides require sub-micron dimensions, which easily leads to intolerable propagation loss due to surface scattering. The smoothness of all etched and polished surfaces becomes an extremely critical factor as the SOI waveguide dimensions approach the sub-micron limit and it is also essential in fabricating thicker ridge waveguides with low propagation and fiber coupling losses.

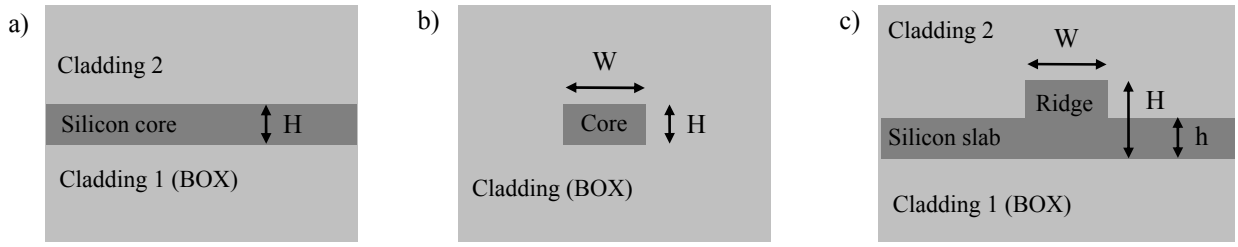

Fig. 1. Schematic cross-sections of three basic SOI waveguide structures: a) slab waveguide (1D), b) rectangular waveguide (2D), and c) ridge waveguide (2D). Dark gray represents the silicon core and light gray represents the cladding materials, which are semi-infinite by default. Silicon core has a height H and a width W. The thickness of the slab surrounding the ridge waveguide is h.

In this paper, theory, simulation results and some experimental results will be represented separately in Chapters 2, 3, and 4 for the above mentioned three basic waveguide structures. Demonstration of very fast (>150 kHz) TO switching in 10 μm thick SOI ridge waveguides is reported in Chapter 5. Finally, the basic principles of the multi-step patterning technology for SOI waveguides are presented in Chapter 6. Throughout the paper, a semi-infinite oxide layer is assumed to surround the silicon core, unless otherwise stated. The material choice for the top cladding has a clear effect on a ridge waveguide's birefringence, as is concluded in Chapter 4. As usual, waveguide modes with the major electric field component aligned horizontally or vertically are labelled TE and TM modes, respectively. The default wavelength is 1550 nm. Most of the experiments are related to approximately 10 μm thick ridge waveguides.

2. SOI SLAB WAVEGUIDES (1D)

To ease the understanding of waveguide modes and the single-mode conditions in SOI waveguides, a brief introduction to the modes in one-dimensional SOI slab waveguides is first presented. A schematic cross-section of the slab waveguide is shown in Fig. 2a. Propagating modes and their effective indices can be easily calculated in this 1D case, for both TE and TM polarization. Two-dimensional SOI waveguide structures (see Chapters 3 and 4) can be approximately analyzed with a so-called effective index method (EIM) by applying the 1D field calculations first in vertical slices of the 2D structure and finally in the horizontal direction (see Fig. 2b).

For simplicity, the following modal analysis is presented only for TE polarization, but the results for TM polarization can be obtained similarly. Calculated effective indices of the first three propagating modes are shown in Fig. 3a as a function of the slab thickness H_{slab}. It can be seen that in several micrometers thick slabs the effective indices have only a slight difference with respect to silicon's refractive index (3.48). When the slab thickness decreases well below 1 μm the effective indices start to decrease rapidly and the modes are cut-off just before their effective indices reach the cladding index (1.46). The cut-off widths for the TE1 and TE2 modes are approximately 250 and 500 nm, respectively. The number of propagating modes N and N^2 are presented in Fig. 3b. Number N increases rapidly with respect to slab

thickness, so that 1 and 10 μm thick slabs already support approximately 5 and 40 modes, respectively. When the waveguide modes are well confined, e.g. when the core dimensions are above 1 μm, the number of modes in a SOI waveguide with a square cross-section can be approximated with N^2. The results in Fig. 3 clearly indicate that SOI slabs and rectangular SOI waveguides must have core dimensions well below 1 μm in order to provide SM operation and that SOI waveguides can have tens or even hundreds of modes already at dimensions below 10 μm.

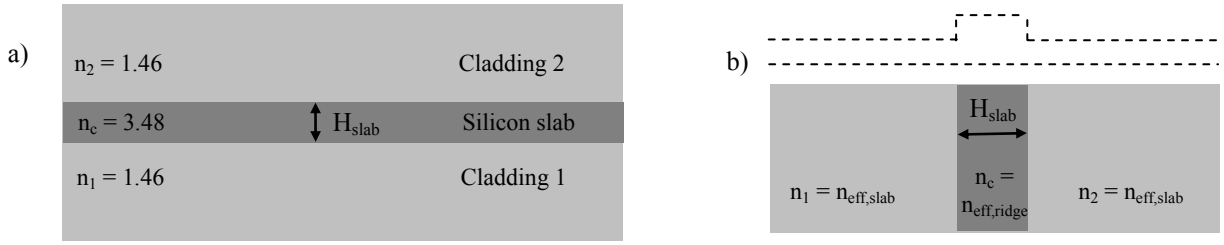

Fig. 2. Schematic cross-section of a 1D SOI slab waveguide with thickness H_{slab}. a) Physical slab structure with a real silicon slab ($n_c = 3.48$). b) Virtual slab structure with calculated effective indices $n_{eff,slab}$ and $n_{eff,ridge}$ as cladding and core indices and H_{slab} equal to ridge width W. This can be used in the effective index approximation of a 2D SOI waveguide, as illustrated by the dashed line.

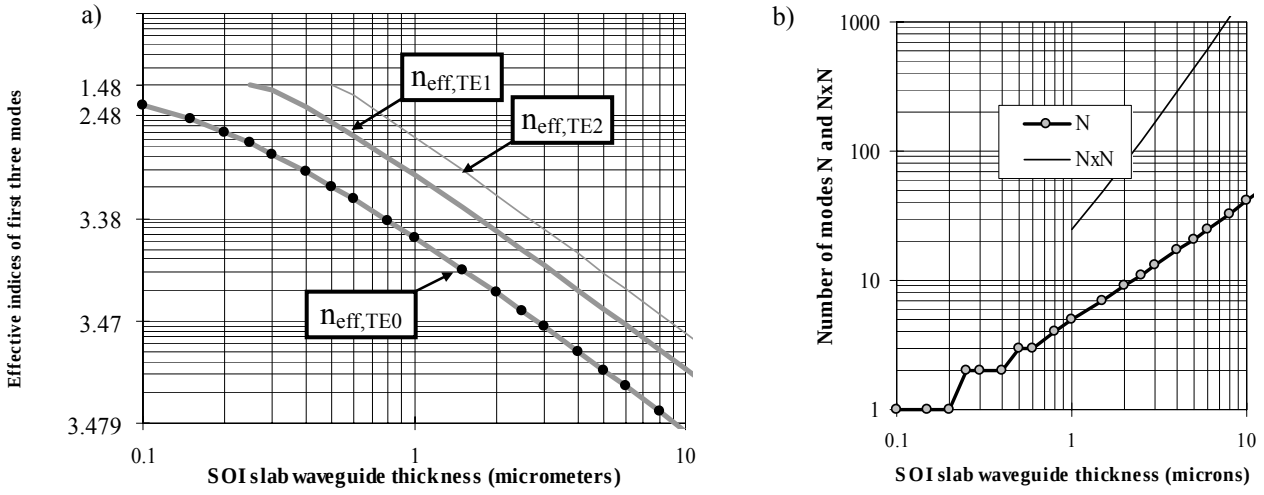

Fig. 3. a) Calculated effective indices of the three lowest TE modes ($n_{eff,TE0 / TE1 / TE2}$) as a function of slab thickness H_{slab} in an SOI slab waveguide. b) Calculated number of propagating waveguide modes N and N^2 as a function of H_{slab}. The latter approximately corresponds to the number of modes in a square waveguide cross-section when the effective index of the mode is close to silicon ($3 << n_{eff} < 3.48$).

The combination of extremely high refractive index difference and dimensions above 1 μm was seen to support many propagating modes in SOI slab waveguides. It also confines the propagating modes very efficiently into the silicon core, except for modes that are very close to cut-off. This can be seen in Fig. 4, where the intensity distributions of three lowest order modes are plotted for slab thicknesses 200 nm, 1 μm and 10 μm. The effective index being close to the core index follows directly from the high confinement, as the effective index can be considered to be an weighted average of the propagation media's refractive index.

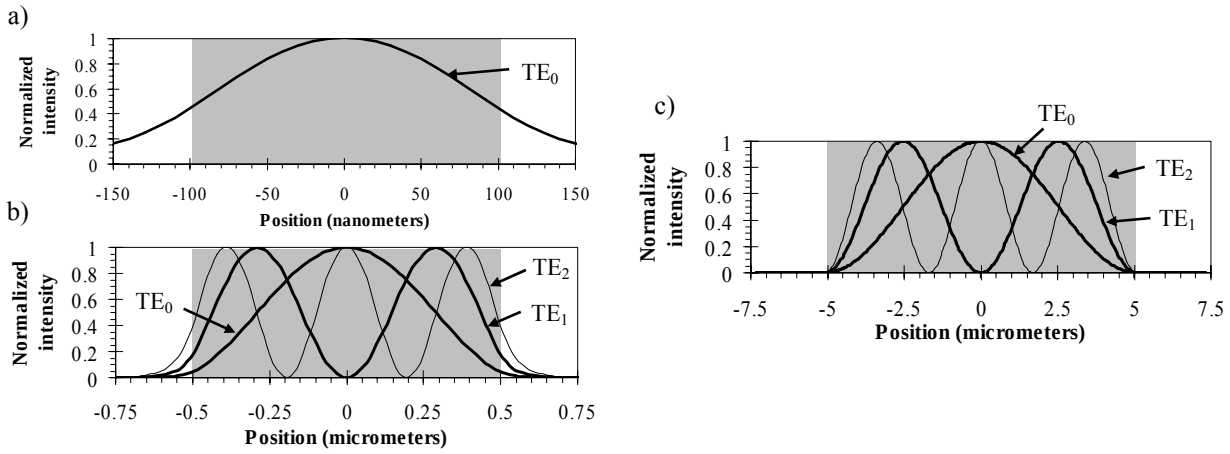

Fig. 4. Calculated intensity distributions of the lowest propagating modes in an SOI slab waveguide with a thickness of a) 200 nm (1 mode), b) 1 μm (5 modes), or c) 10 μm (>40 modes). The gray area illustrates the silicon slab.

3. RECTANGULAR SOI WAVEGUIDES

First theoretical approximation for rectangular SOI waveguides can be based on the effective index method. If the dimensions are well above 1 μm the problem of finding waveguide modes is sufficiently separable with respect to the horizontal and vertical directions. Then the results from Chapter 2 can be readily used to estimate the modal behavior in rectangular waveguides. Based on such an analysis, it can be stated that the rectangular SOI waveguides are multi-moded unless the core dimensions are clearly below 1 μm and that the number of modes increases very rapidly with respect to the dimensions. The fundamental mode is extremely well confined into the silicon core, which leads to some favorable characteristics. For example, the rectangular waveguides can have ultra-small bending radii of a few micrometers[11] and they can even make abrupt changes of course based on total internal reflection (TIR) in so-called waveguide mirrors, as depicted in Fig. 5. With an air or oxide cladding, TIR mirrors can turn the SOI waveguides by more than 90°. Also, arrays of rectangular SOI waveguides can be packed very densely without the risk of any optical or thermal cross-talk between them. This allows for very high miniaturization of PICs on SOI substrates.

Further on, the very high number of modes can be utilized in interferometric components, such as multi-mode-interference (MMI) couplers. The length of an MMI coupler increases with respect to the second power of its width, and the width is limited by the need for a sufficient number of horizontal waveguide modes. In weakly guiding structures a 2×2 MMI coupler's length is typically from a few hundred micrometers to a few millimeters. A rectangular SOI waveguide only needs to have a width of 2.5 μm to support more than 10 horizontal modes. This can lead to MMI couplers with lengths well below 50 μm, enabling very compact PICs.

The very high index difference also poses some important problems that must be solved. Rectangular SOI waveguides tend to be very multi-moded, which seriously limits their applicability e.g. in optical telecommunication and in many interferometric devices. This problem can be tackled by reducing the dimensions of the waveguide to the SM region, but this severely increases scattering losses. A better solution could be to couple light adiabaticly from SM waveguides to rectangular waveguides and back, so that higher order modes are not excited to any relevant extent. This is difficult to realize with traditional waveguide technologies, but it can be obtained with the above mentioned multi-step patterning principle, as is explained in Chapter 6.

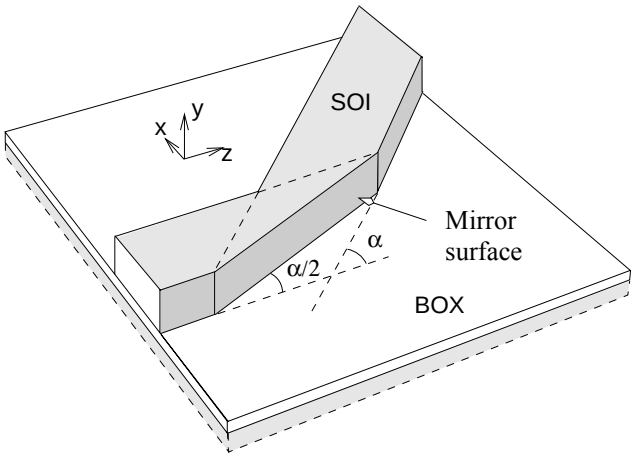

Fig. 5. Schematic view of an abrupt waveguide mirror, which produces total internal reflection between the silicon core and the surrounding cladding (e.g. air or silicon dioxide) and, thus, turns the waveguide by angle α.

Accurate analysis of the rectangular SOI waveguides requires the use of numerical analysis, especially when the core dimensions are close to the single-mode region. Rigorous numerical simulations were applied in a study of modal properties in rectangular SOI waveguides. Simulations were carried out with a commercial software package (*TempSelene* v.4.3) from Kymata Netherlands (currently represented by C2V). The applied algorithm (*BendSolver*) is full-vectorial and capable of calculating both propagating and lossy modes. Simulations verified that the effective index approximation is not valid close to the SM region. The SM limit for a square core was found to be approximately W = H = 350 nm. On the other hand, the SM limit for W was found to be as high as 500 nm for a 250 nm thick silicon core. Calculated intensity distributions of the TE_{00} and TM_{00} modes in three different waveguide cross-sections are presented in Fig. 6. Strong polarization dependency can be clearly observed when the dimensions are reduced beyond the SM limit.

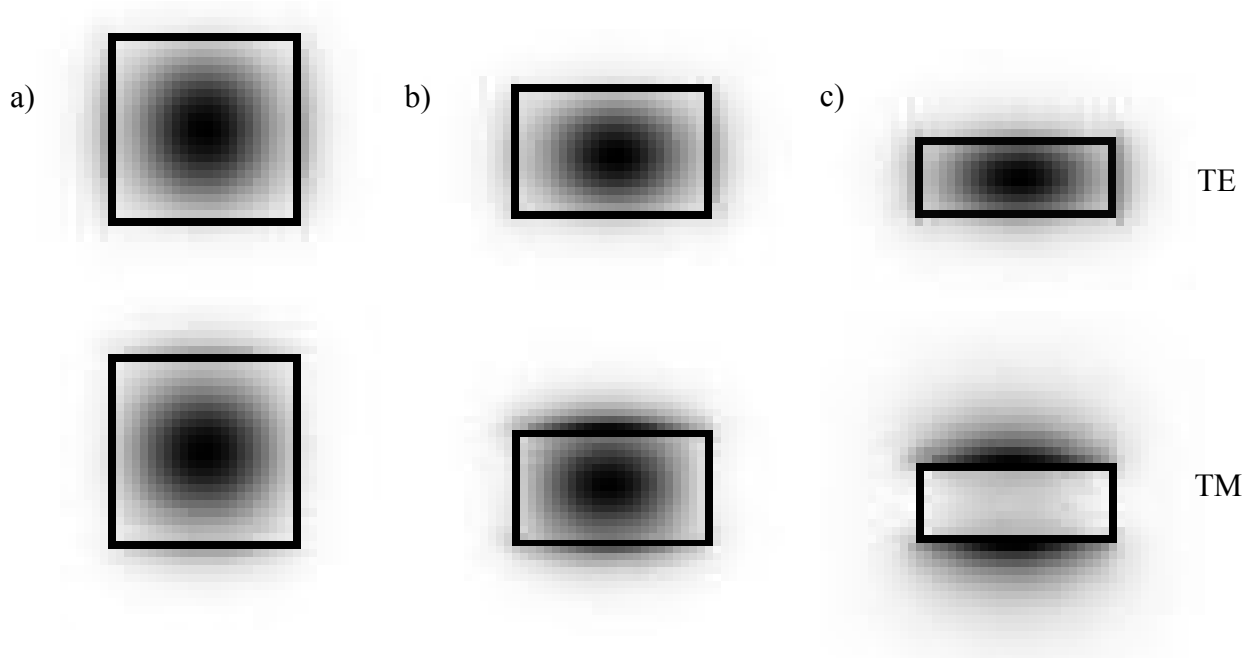

Fig. 6. Simulated intensity distributions of rectangular SOI waveguides separately for TE and TM polarization when the waveguide width is 500 nm and the waveguide height is a) 500 nm, b) 350 nm, or c) 200 nm.

4. SOI RIDGE WAVEGUIDES

4.1 Theory and simulation of ridge waveguides

Ridge type SOI waveguides can be single-moded with both width and height clearly above 10 μm. It should be noted that ridge waveguides are sometimes also referred to as "rib" or "partially etched" waveguides. The thickness of the silicon layer is H within the ridge and h around the ridge. A schematic cross-section of the SOI ridge waveguide with a contour plot of the fundamental mode's intensity distribution is shown in Fig. 7.

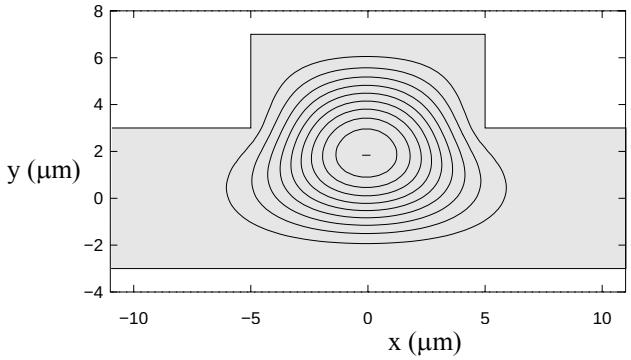

Fig. 7. Schematic cross-section and a calculated intensity distribution of the fundamental mode in a ridge waveguide (H = 10 μm, h = 6 μm, W = 10 μm).

With certain H and h the width W of the ridge is limited by a single-mode condition

$$\frac{W}{H} < 0.3 + \frac{h/H}{\sqrt{1-(h/H)^2}}, \tag{1}$$

as proposed by Soref[4]. This width limitation essentially eliminates the higher order horizontal modes. In practice it assures that the effective index (e.g. $n_{eff,TE10}$) of any higher order horizontal mode in the 2D ridge waveguide is lower than the effective index ($n_{eff,TE0}$) of the fundamental mode in the 1D slab waveguide surrounding the ridge. Thus, all higher order horizontal modes see a negative effective index difference in the horizontal direction and, therefore, leak to the surrounding slab waveguide[10]. On the other hand, propagation of higher order vertical modes is prevented by choosing[4]

$$h/H \geq 0.5. \tag{2}$$

This assures that the lowest intensity maximum of any higher order vertical mode has a negative or zero effective index difference in the horizontal direction and such a mode is always radiative[10]. When the SM limit is approached both horizontal and vertical higher order modes spread into the silicon slab and start to radiate power along the slab away from the ridge. The 1D slab offers these modes an escape port in a similar fashion as a traditional (2D) cladding offers for optical fibers and typical low-index contrast silica waveguides.

According to the effective index approximation, the large refractive index difference is replaced by a much smaller effective index difference in the horizontal direction. As a result, the bending of SM ridge waveguides becomes much more difficult and typically requires a bending radius of several millimeters to avoid harmful bending losses. The strong asymmetry between the horizontal and the vertical direction also tends to cause some geometrical polarization dependency. In particular, the ridge waveguides can be birefringent and the propagation losses in straight and, especially, in curved waveguides can be polarization dependent, as is discussed later.

The two limitations (1-2) together, as proposed by Soref, form a sufficient, but not an exclusive single-mode condition. Single-mode operation can be obtained also when $h/H < 0.5$ if the ridge is sufficiently narrow. Therefore, a detailed analysis of the single-mode conditions was carried out for 10 and 3 μm thick SOI ridge waveguides by using various thickness ratios in the range $0.25 \le h/H \le 0.8$ and by varying the ridge width W in order to locate the maximum width W_{max} for SM operation.

The SM analysis of ridge waveguides was based on rigorous calculations with the above mentioned *TempSelene* simulation software and the same full-vectorial algorithm. All the relevant higher order modes radiate along the silicon slab, so transparent boundary conditions only need to be used in the horizontal direction. Six to ten perfectly matched layers (PMLs) per boundary were used in the horizontal direction to allow higher order modes to spread and radiate into the silicon slab. The calculation grid size was varied between 128×64 and 256×64 and the width of the calculation area was varied between 4 and 8 times H. The rejection of the higher order modes was made by using several different requirements that had to be valid for any propagating mode. The intensity maxima were required to reside below the ridge, the intensity distribution was not allowed to significantly spread out of the calculation area and no significant losses were accepted. These criteria are somewhat dependent on the simulation parameters and, therefore, some results were positioned into a so-called gray-area, instead of putting all the results either to SM or MM region. The true SM limit is expected to lie somewhere within the gray-area. The results are shown in Figs. 8 and 9.

When $0.25 < h/H < 0.4$, the suppression of horizontal TE_{10} and TM_{10} modes requires that W is somewhat smaller than the Soref's maximum width (1). In the same h/H range the elimination of vertical TE_{01} and TM_{01} modes poses a much more strict width limit. SOI ridge waveguides can be SM even when $h/H < 0.3$, but this requires very narrow ridges. At $h/H = 0.3$, for example, 10 and 3 μm thick waveguides are SM when the ridge widths are below 3 and 1 μm, respectively. It should also be noted that higher order vertical modes may appear also when $h/H > 0.5$ if the ridge is sufficiently wide.

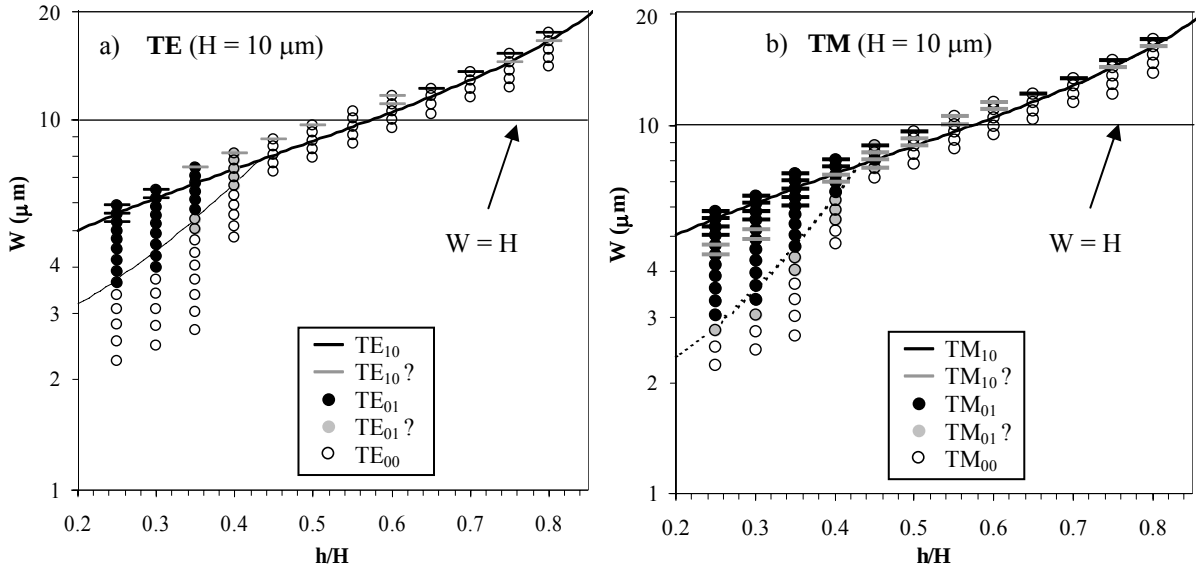

Fig. 8. Simulated SM conditions for 10 μm thick SOI waveguides, separately for a) TE and b) TM polarization. Thick continuous lines represent the maximum width according to Soref's rule, while the thin dashed line represents a new width limit for eliminating the TE_{01} and TM_{01} modes. Circles define simulated structures. Horizontal lines and filled circles indicate higher order horizontal (TE_{10} and TM_{10}) and vertical (TE_{01} and TM_{01}) modes, respectively. Gray color indicates the gray-zone between clearly SM and MM regions.

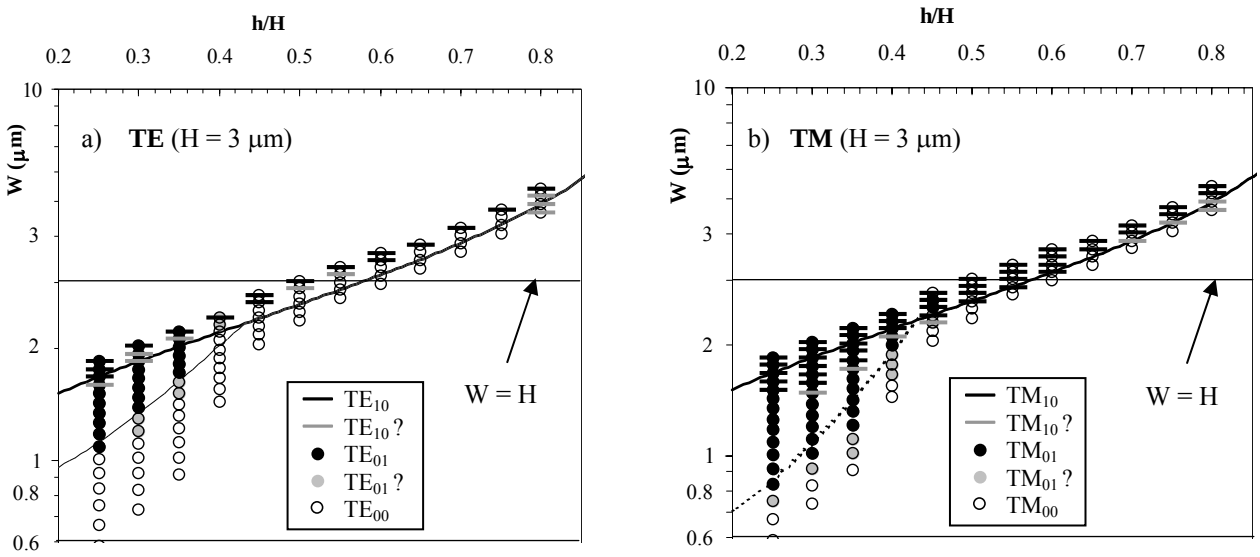

Fig. 9. Simulated SM conditions for 3 µm thick SOI waveguides, separately for a) TE and b) TM polarization. Symbols as in Fig. 8.

As can be seen from Figs. 8 and 9, the SM condition of SOI ridge waveguides is slightly polarization dependent. The waveguides also have a small geometrical birefringence $\Delta n = |n_{eff,TE} - n_{eff,TM}|$ that depends on H, h and W. In typical waveguide structures with H ≈ 10 µm the simulated birefringence is below $5 \cdot 10^{-5}$, but in 1.5 µm thick SOI waveguides it can be as high as $5 \cdot 10^{-3}$.

4.2 Theory and simulation of bends in ridge waveguides

Perhaps the greatest limitation of ridge waveguides is their tendency to cause large bending losses to the propagating light. For example, both measurements and simulations[12] have shown, that in a 10 µm thick ridge waveguide with etch depth of 5 µm, bending radii smaller than 2 cm cause significant losses. This means that high integration densities in PICs are very hard to achieve with thick waveguides.

The amount of bending loss in several bent ridge waveguides was calculated by the same *BendSolver* algorithm as described above. As *TempSelene* can calculate the mode fields in the cylindrical coordinate system, there is no need to use any approximative methods, such as conformal mapping. The software can readily calculate the loss per unit length from the complex propagation constant β that accompanies every mode field. Three waveguides with thicknesses H of 10 µm, 3 µm and 1.5 µm, all with etch depth of H/2, were considered. The Soref's SM condition (1) was used to determine the ridge widths W, resulting in values of 8.8 µm, 2.6 µm, and 1.3 µm, respectively. The calculation parameters used were essentially the same as those given in subsection 4.1. Results from the calculations are presented in Fig. 10.

From the results it can be seen, that bending losses are high for the 10 µm thick ridge waveguide, but that they diminish rapidly as the waveguide is made smaller. Further reduction to the bending loss can be obtained by using larger ridge widths than the ones given by Soref's equation, or by using deeper than H/2 etched waveguides. Despite these alterations to the geometry, the waveguide can still operate in the SM region, because higher order modes are more susceptible to radiate away from the ridge. Finally, it should be noted that the bending loss has a very strong polarization dependency.

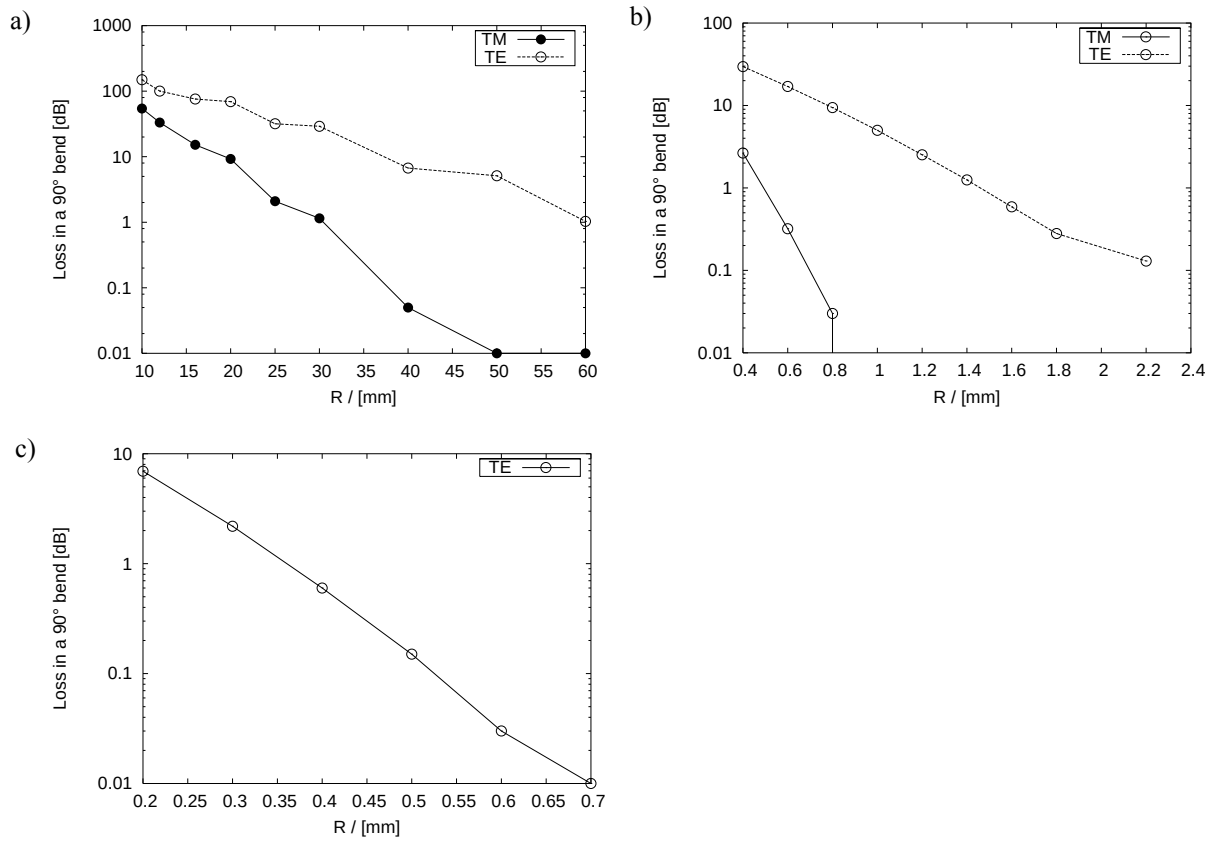

Fig. 10. Simulated bending losses for standard ridge waveguides with thickness H equal to a) 10 μm, b) 3 μm and c) 1.5 μm.

4.3 Fabrication and measurements

Several different waveguides were fabricated with thickness H typically in the range of 8 to 10 μm, etch depth H–h ≈ H/2, width W ranging from 6 to 14 μm and cladding material being thermal oxide (TOX), low-temperature oxide (LTO), TEOS oxide or air (i.e. no cladding). The BOX thickness of the bonded SOI wafers was 1 μm. The waveguide structures were patterned with standard UV-lithography. An oxide hard mask was used for etching the waveguide structure into silicon by inductively coupled plasma (ICP). In the very beginning of the waveguide etching process continuous etching was used. Then the etching continues with alternating passivation and etching steps (etching gas SF_6, passivation gas C_4F_8) to ensure side-wall verticality. The durations of the etching and passivation cycles were both 5 s. After the removal of the residual mask TOX, LTO or TEOS cladding was optionally grown on top of the waveguide. Finally, the waveguides were diced into chips and the endfacets were polished to optical quality.

One problem of characterizing SOI waveguides is to perform accurate propagation loss measurements, since the total propagation loss is comparable to the insertion and coupling losses in short waveguides. Therefore, up to 72 cm long spiral waveguides with bending radii varying between 27 and 42 mm were fabricated to measure the propagation losses accurately. In the measurement setup the laser light was polarized and butt-coupled into a waveguide with polarization-maintaining fiber (PMF). One axis of the PMF was aligned parallel to the chip surface, i.e. horizontally. This ensured that the polarization modes of the input fiber were coupled directly to the polarization modes of the waveguide with minimum cross-talk (below –25 dB). The transmitted light was coupled into a multimode fiber (MMF) and guided to a detector. The setup enabled transmission measurements for both TE and TM polarization. A fiber-to-fiber reference transmission was measured by directly butt-coupling the PMF and MMF. To obtain an exact value for the excess loss of

a waveguide, both the Fresnel reflection loss 3 dB (including both facets) and the theoretical fiber-to-waveguide modal coupling loss (only input facet) were subtracted from the insertion loss.

The measured propagation loss for a 14 μm wide SM spiral waveguide was 0.30±0.05 dB/cm for both TE and TM polarization. It is expected that this loss is still somewhat effected by the spiral bends and that an equally long straight waveguide would provide a lower loss value. However, the roughness of the waveguide side-walls still has the greatest contribution to the measured loss.

The birefringences of the waveguides were measured using the fixed analyzer method[13]. The experimental measurement setup is shown in Fig. 11. Light from a broadband light source was polarized and butt-coupled into the waveguide with a PMF. Polarization axis of the PMF was rotated so that light polarized at a 45° angle was launched into the waveguide. Optical powers coming out of the waveguide in two orthogonal linear polarization states ±45° were measured with a rotatable polarizer as a function of wavelength by using an optical spectrum analyzer. Either one spectrum or a ratio of the two spectra (polarization extinction ratio, PXR) could be used to calculate the birefringence. Waveguide birefringence induces a periodic transmission (or PXR) curve as a function of frequency. The period is equivalent to a phase difference of 2π (one beat length). The birefringence Δn can be calculated using equation

$$\Delta n = m\frac{c}{\Delta f\, L} = m\frac{\lambda_1\lambda_n}{\Delta\lambda L}, \tag{3}$$

where m represents the number of periods included in a frequency range Δf, or a corresponding wavelength range $\Delta\lambda = \lambda_n - \lambda_1$, between two transmission (or PXR) maxima (λ_1 , λ_n) and L is the length of the waveguide.

Main problem of the method is that wavelength dependence of the birefringence has an effect on the results, especially when the birefringence is low, because measurements require the use of a broad spectrum. However, wavelength dependence was not observed in our SOI waveguide measurements in the wavelength range from 1350 to 1600 nm.

Figure 12a shows measured PXR spectra from straight waveguides with LTO and TEOS claddings. Periodic response of the transmission signal is well seen in the case of LTO. Birefringence value of $6\cdot10^{-4}$ was obtained using equation (3). It can be seen that TEOS cladding produces a clearly lower birefringence than LTO. Approximately one half of a period is seen in the TEOS spectrum, which lead to an estimated birefringence of $1\cdot10^{-4}$. The fixed analyzer method could not provide an accurate birefringence value for a waveguide with air cladding because the associated spectrum showed less than one half of a period, which indicates a birefringence of less than $1\cdot10^{-4}$. Measured birefringence for a straight waveguide with TOX cladding was similar to the results for LTO and it is shown in Fig. 12b as a function of W. A maximum of $6.8\cdot10^{-4}$ and a minimum of $1.5\cdot10^{-4}$ were obtained with waveguide widths 6 and 2 μm, respectively.

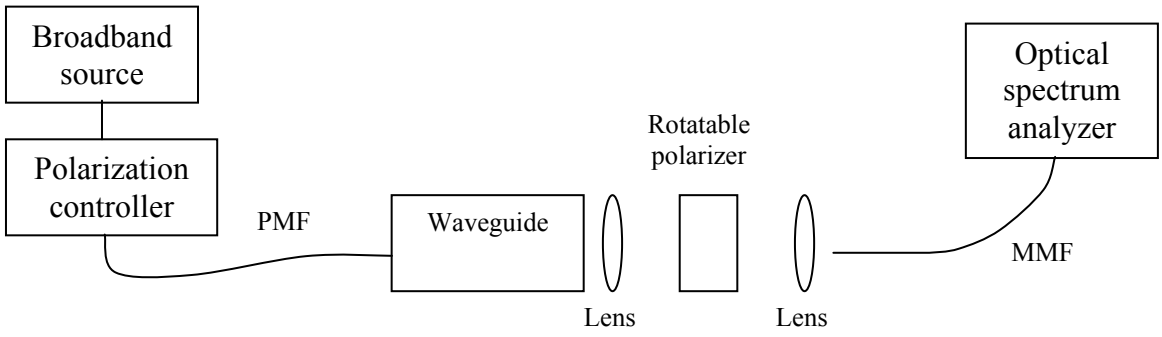

Fig. 11. Measurement setup used to determine waveguide birefringencies.

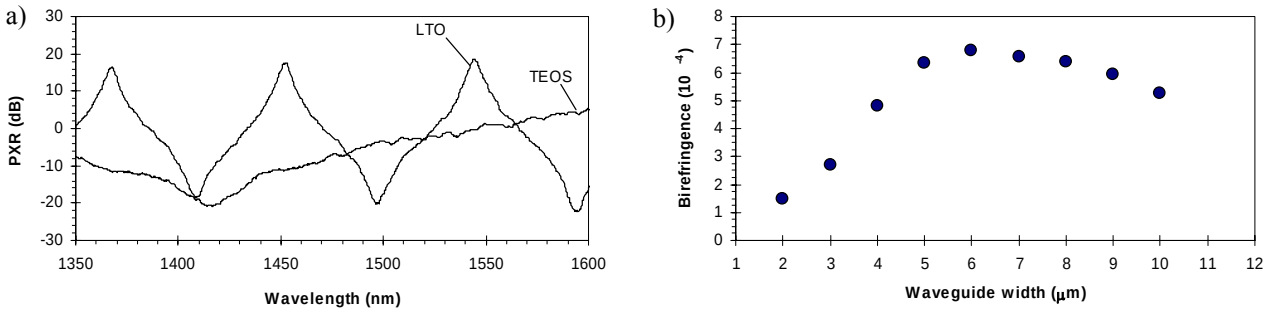

Fig. 12. a) Measured PXR spectra from two 4 cm long waveguide samples with LTO and TEOS claddings (H ≈ 9 μm, W = 8 μm). b) Measured birefringence as a function of waveguide width in a 71 mm long sample chip with TOX cladding (H ≈ 9 μm).

5. THERMO-OPTICAL SWITCHING IN SOI RIDGE WAVEGUIDES

Typical TO switches made from silica or polymers typically have a maximum frequency below 1 kHz. This is mostly due to their poor thermal conductivity, relatively large core size and thick cladding, which is necessary to optically insulate the waveguide from the heating electrode. Thick SOI ridge waveguides have good thermal conductivity and a thin top cladding between the heating electrode and the silicon core. These characteristics lead to faster switching operating, but also to a somewhat higher power consumption than what is seen in the well insulated and slow switches.

To study the potential of SOI waveguides in optical switching, a TO switch based on a 9 μm thick SOI ridge waveguide was fabricated and characterized. The switch was implemented by using a 2x2 Mach-Zehnder interferometer (MZI) layout and it was operated by using both conventional square wave modulation and a new interferometric modulation technique. The cross-section of the SOI waveguide with an aluminum heater on top is shown in Fig. 13a. Detailed design and fabrication of the switch are published elsewhere[14,9]. The switch is in a cross state (off), when the heating elements are not operated. It turns into a bar state (on) when a temperature difference corresponding to a phase difference of $\Delta\phi$ = 180° is applied between the two waveguide branches by operating at least one of the heaters. The optimum bar- and cross-states can be obtained only when the directional couplers (DCs) are identical and their lengths correspond to perfect 50:50 (-3 dB) power division.

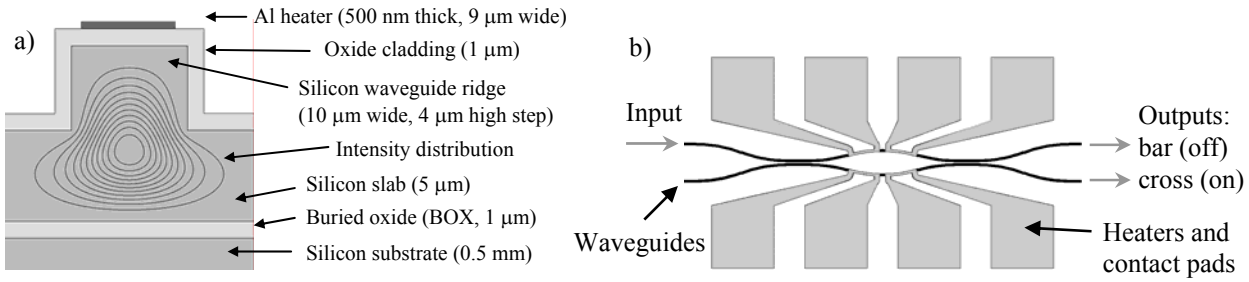

Figure 13. a) Cross-section of a SOI ridge waveguide with an aluminum heater on top of the ridge. The intensity distribution of the fundamental mode is again shown with contour lines. b) A schematic layout (top-view) of the 2x2 MZI switch.

Before carrying out the switching measurements, the switches were characterized optically without heating them. This showed strong polarization dependency and slightly non-ideal DC lengths. Therefore, all the following results are obtained with TE polarized input light and the switches have a maximum extinction ratio (ER) of 17 dB (98:2). During

the switching, this is an optimum value that represents perfect phase modulation. The polarization dependency and the ER can be improved without a significant change in the modulation frequency. The heating power P in the active waveguide branch was then adjusted to P_{on} so that a static on-state was optimized, resulting in $P = P_{on} = 300$ mW. The maximum frequency for full phase modulation (~99%) with $P = P_{on}$ was approximately 10 kHz. For lower phase modulation depths, e.g. 90% or 50%, the frequency can be clearly above 10 kHz. This already represents an order of magnitude improvement with respect to commercial TO switches.

The details of the new modulation method are presented elsewhere[9], but the basic principle is explained in the following and presented in Fig. 14a. Instead of heating just one waveguide branch, both branches of the MZI are used for heating. In the off state they are heated with equal power, while in the on state only one of the branches is heated. Further on, both the rise and fall time are remarkably shortened by applying a high heating power peak to the other branch and by dropping the heating power of the other branch to zero. The new method increases the frequency very efficiently with respect to power consumption and it can be applied to increase the operational frequency or the response time of other interferometric components as well. In case of the fabricated SOI switch, the switching speed was pushed up to 167 kHz. This was the maximum for the very simple and inexpensive control electronics used. Even at 167 kHz the ER was still better than 13 dB (95:5), i.e. close to the optimum. Average total heating powers were 120 mW and 350 mW during off- and on-states, and 760 mW and 1.13 W during the 3 μs long fall- and rise-times, respectively. In random modulation all alternatives are equally popular and the average heating power is 590 mW.

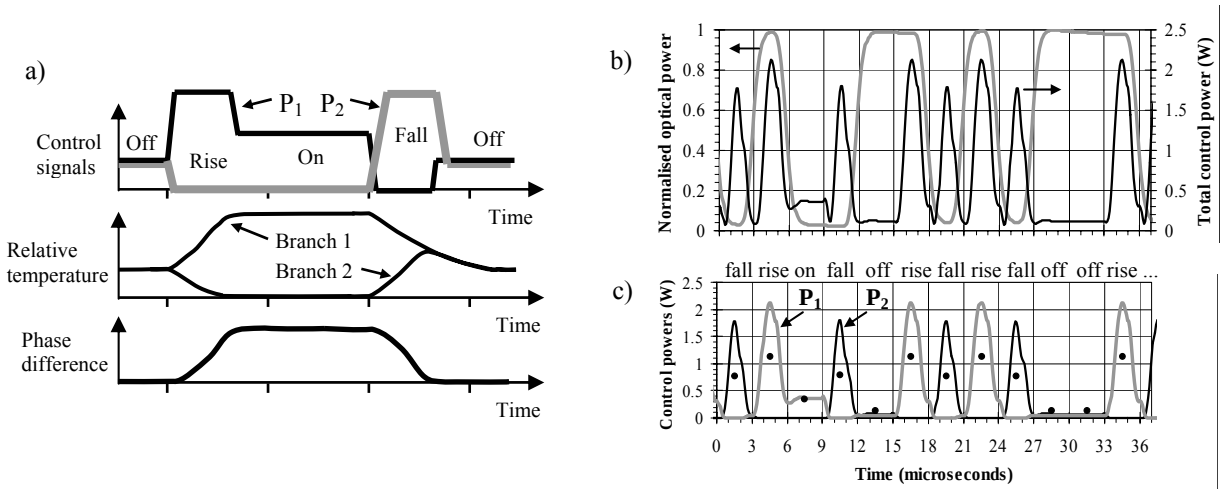

Fig. 14. a) Schematic principle of the new modulation method. Measured results at 167 kHz: b) Optical response (cross-state output) and total heating power. c) Heating powers of the two branches (P1, P2), and an average power for every 3 μs time span (black dots). Optical signal has a 2 μs delay with respect to P1 and P2 (labels on top refer to heating pulses).

6. MULTI-STEP PATTERNING OF SOI WAVEGUIDES

Traditionally, optical waveguides are patterned by using a single mask layer. Other mask layers may be used to define heaters etc, but typically they do not contribute to the basic waveguiding. Using a single mask layer to define optical waveguiding is sufficient for most applications and it is much more simple to realize than aligning different mask layers with respect to each other with the required accuracy.

However, the use of more than one mask layer in the patterning of a single SOI waveguide cross-section has significant advantages, as is explained in the following. The principle is called multi-step patterning and its potential is illustrated by presenting four different SOI waveguide structures that have significant advantages over traditional waveguides. The

main advantages of these multi-step waveguides are the potential for extreme miniaturization and the ability to efficiently couple light between different types of waveguides and fibers.

First, two different structures for converting a ridge waveguide into a rectangular waveguide (or vice versa) are shown. For simplicity, only two mask layers have been used. However, one can also use more mask layers, either in a single waveguide cross-section or by connecting waveguides with different mask layer pairs, one after another. The two structures are schematically presented in Fig. 15. The first transformation occurs between a ridge waveguide and a smaller rectangular waveguide, while the second transformation involves ridge waveguides and rectangular waveguides of equal height. Both of them can be used to combine the advantages of ridge waveguides (SM, thick, low loss) and rectangular waveguides (tight bends, mirrors, short MMIs).

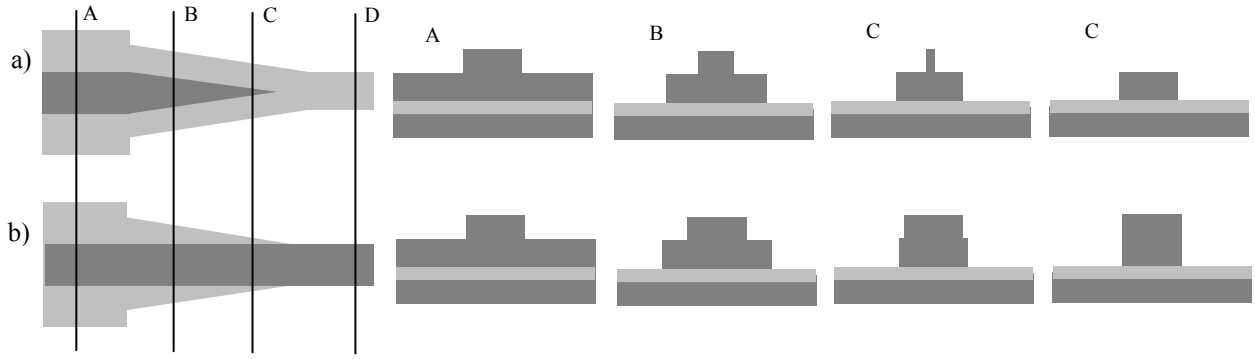

Fig. 15. Two different 3D waveguide tapers between a rectangular and a ridge waveguide. The height of the ridge is a) greater than or b) same as the height of the rectangular waveguide. The layouts on the left describe the structures as seen from the top and the cross-sections A, B, C and D are shown on the right.

The changing of the waveguide cross-sections must be carried out adiabatically, i.e. in a sufficiently small angle with respect to propagation. Depending on the type and the size of the waveguide, this may require relatively long tapering areas, such as tens or even hundreds of micrometers. The alignment between the mask layers must be carried out accurately, but the alignment tolerances can be partially relaxed by using appropriate processing steps. In the 3D tapers shown in Fig. 15 the definition of the waveguide can be transferred from one mask layer to another, so that both mask layers have a relevant contribution to the waveguiding only in the tapering region. The sharp tip in Fig. 15a will have a finite width due the finite lithographic resolution. However, according to the simulations the effect of the tip on the fundamental mode becomes negligible when the tip width becomes much smaller than the width and the height of the underlying rectangular waveguide. It should be noted that these 3D tapers also allow for efficient coupling between a PhC waveguide and a SM ridge waveguide. In the miniaturization of PICs the input waveguides and local mode strippers can be formed of SM ridge waveguides, while the bends, waveguide mirrors, couplers and other such structures can be realized densely with small rectangular waveguides.

The third type of transformation connects two ridge waveguides that have different heights. This transformation is described schematically in Fig. 16. It shows a similar sharp tip as in Fig. 15a, but also here the finite width of the tip becomes negligible with a sufficiently wide shallow ridge. The main application of this structure is to change the height of a waveguide without losing the SM behavior. Several successive tapers can be used to obtain very large height differences. Larger waveguides are especially useful for low-loss propagation of longer distances and for coupling with hybrid integrated waveguides, fibers and lasers. The smaller waveguides, on the other hand, are better for realizing ultra-small PICs and fast modulators or switches.

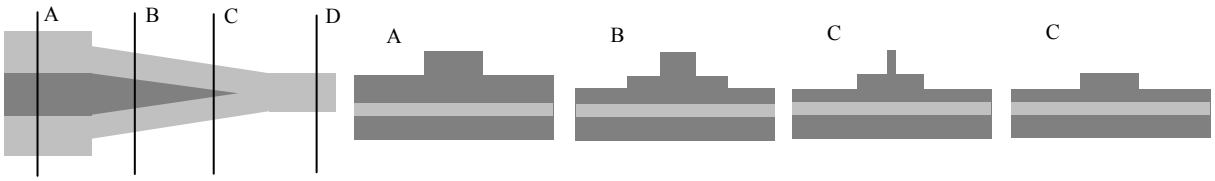

Fig. 16. A 3D waveguide taper connecting two ridge waveguides with different heights. The layout on the left describes the structure as seen from the top and the cross-sections A, B, C and D are shown on the right.

The fourth example of multi-step SOI waveguides is an asymmetric bend. By etching a shallow groove next to the SM waveguide ridge the effective index difference of the fundamental mode can be locally increased. This allows to realize small waveguide bends without forcing the waveguide to MM operation. The distance and width of the groove can be tuned along the bend to obtain an optimum for the transmission without launching the higher order modes. A schematic layout of the structure is shown in Fig. 17, together with contour plots of the fundamental mode. It can be clearly seen that the very high bending loss of the ridge waveguide can be completely suppressed by using the groove.

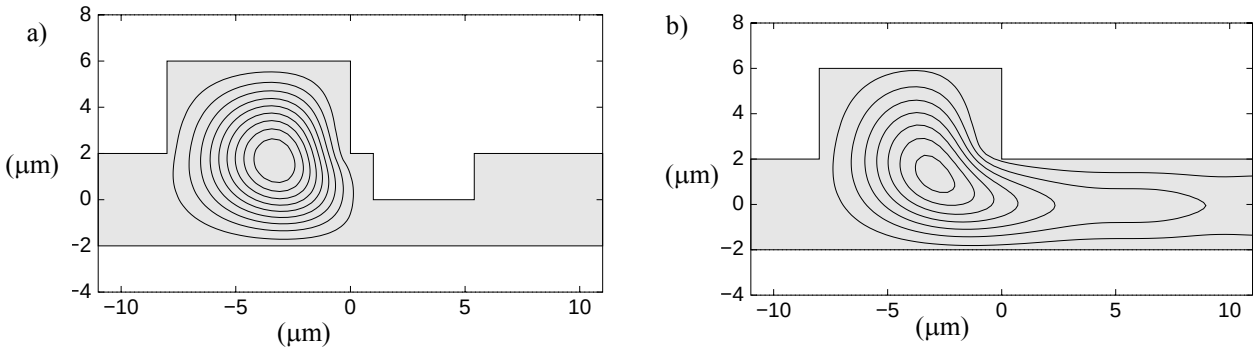

Fig. 17. Cross-sections and calculated intensity distributions of SOI waveguides with a bending radius of 10 mm a) with and b) without an additional groove.

According to the simulations[12] carried out in this work there is a lot of potential in realizing extremely compact optical circuits based on multi-step SOI waveguides. The use of additional etch steps requires the use of additional lithography masks and process steps, but the advantages should clearly overcome the associated extra efforts in fabrication. The basic principle of multi-step patterning can be applied to thick (e.g. 10 μm) as well as thin (e.g. 1 μm) waveguides.

7. CONCLUSIONS

Silicon-on-insulator waveguide technology has strong potential in providing ultra-compact, highly efficient and low-cost PICs in the future. Further development of the fabrication technology will shortly provide the means to realize efficient coupling from standard fibers and thick SOI ridge waveguides to very thin SOI waveguides (ridge or rectangular) as well as to photonic crystal structures fabricated in SOI. The high bending losses in thick SOI waveguides can be eliminated by applying additional grooves to the outer sides of the waveguide bends. Waveguide arrays and devices such as MMI couplers and switches can be made very small by taking advantage of the excellent confinement and high number of modes in rectangular waveguides. The advantages of SOI technology become more and more apparent when the integration and miniaturization level of PICs is increasing. It will have applications not only in optical telecommunication, but also in optical interconnections and, perhaps, in sensor technologies as well.

When developing the SOI waveguide technology one must keep the roughness of the etched silicon surfaces very small to avoid any significant scattering losses and the roughness must even be reduced from the present values when the waveguides dimensions are reduced to the sub-micron range. However, the present SOI waveguide technology can already provide losses that are competitive with other waveguide technologies, such as the 0.3 dB/cm propagation loss measured from bent waveguides within this work. Waveguide birefringence is also an important issue, especially in small waveguides, and the selection of an appropriate cladding material appears to be crucial in keeping it low.

ACKNOWLEDGEMENTS

This work was partly supported by The European Space Agency under ESTEC Contract Number 17703/03/NL/PA and Tekniikan Edistämissäätiö (Technology Development Fund, Finland). Markku Rönö, Kimmo Solehmainen, and Kai Kolari are acknowledged for their valuable contribution to the work.

REFERENCES

1. B. Jalali, "Silicon-on-insulator photonic integrated circuit (SOI-PIC) technology", *SPIE Proc.* **2997**, pp. 60-71, 1997.
2. K. Hosomi, T. Katsuyama, "A dispersion compensator using coupled defects in a photonic crystal", *IEEE J. Quantum Electron.* **38**, pp. 825-829, 2002.
3. S. Yliniemi, T. Aalto, P. Heimala, P. Pekko, K. Jefimovs, J. Simonen, T. Uusitupa, "Fabrication of photonic crystal waveguide elements on SOI", *Proc. SPIE* **4944**, pp. 23-31, 2003.
4. R. A. Soref, J. Schmidtchen, K. Petermann, "Large single-mode rib waveguides in GeSi-Si and Si-on-SiO_2", *IEEE J. Quantum Electron.* **27**, pp. 1971-1974, 1991.
5. T. Zinke, U. Fischer, B. Schüppert, K. Peterman, "Theoretical and experimental investigation of optical couplers in SOI", *Proc. SPIE* **3007**, pp. 30-39, 1997.
6. P. D. Trinh, S. Yegnanarayanan, F. Coppinger, B. Jalali, "Silicon-on-insulator (SOI) phased-array wavelength multi/demultipelexer with extremely low-polarization sensitivity", *IEEE Photon. Technol. Lett.* **9**, pp. 940-942, 1997.
7. T. Aalto, S. Yliniemi, P. Heimala, P. Pekko, J. Simonen, M. Kuittinen, "Integrated Bragg gratings in silicon-on-insulator waveguides", *Proc. SPIE* **4640**, pp. 117-124, 2002.
8. A. Cutolo, M. Iodice, A. Irace, P. Spirito, L. Zeni, "An electrically controlled Bragg reflector integrated in a rib silicon on insulator waveguide", *Appl. Phys. Lett.* **71**, pp. 199-201, 1997.
9. T. Aalto, M. Kapulainen, S. Yliniemi, P. Heimala, and M. Leppihalme, "Fast thermo-optical switch based on SOI waveguides", *Proc. SPIE* **4987**, pp.149-159, 2003.
10. T. Aalto, P. Heimala, S. Yliniemi, M. Kapulainen, and M. Leppihalme, "Fabrication and characterization of waveguide structures on SOI", *Proc. SPIE* **4944**, pp.183-194, 2003.
11. A. Sakai, T. Fukazawa, T. Baba, "Low loss ultra-small branches in a silicon photonic wire waveguide", *IEICE Trans. Electron.* **E85-C**, pp.1033-1038, 2002.
12. M. Harjanne, T. Aalto, "Design of tight bends in silicon-on-insulator ridge waveguides", Accepted for publication in *Physica Scripta*
13. Y. Namihira, J. Maeda, “Comparison of various polarisation mode dispersion measurement methods in optical fibres”, *Electron. Lett.* **28**, pp. 2265-2266, 1992.
14. T. Aalto, P. Heimala, P. Katila, "Integrated optical switch based on SOI-technology", *Physica Scripta* **T79**, p. 123-126, 1999.